

The origin of spongy texture in minerals of mantle xenoliths from the Western Qinling, central China

Ben-Xun Su · Hong-Fu Zhang · Patrick Asamoah Sakyi · Yue-Heng Yang ·
Ji-Feng Ying · Yan-Jie Tang · Ke-Zhang Qin · Yan Xiao · Xin-Miao Zhao ·
Qian Mao · Yu-Guang Ma

Received: 10 October 2009 / Accepted: 1 June 2010 / Published online: 25 June 2010
© Springer-Verlag 2010

Abstract Spongy textures are observed in mantle peridotite xenoliths hosted in Cenozoic kamacites from the Western Qinling, central China. These textures are mainly developed in clinopyroxenes and spinels, and occur as spongy rims consisting of low-Na clinopyroxene, ilmenite, and bubbles, enclosing nonspongy cores. The ilmenites and bubbles exhibit shapes and sizes that vary with the width of the spongy rims. The spongy-textured minerals preserve primary shapes and well-defined grain boundaries and do not show apparent interaction with contact minerals or observed melts except the subsequent melts forming melt pockets. The xenocrysts display reactive zoning textures with host magmas rather than spongy textures. Compositionally, the spongy rims are enriched in Ca, Ti, and most trace elements, have high Cr#, and are depleted in Na, Al, Fe, Al^{VII}, and Al^{IV}/Al^{VII} compared with the cores. These

observations suggest that melts/host magmas did not play any significant role in the formation of the spongy textures. We therefore propose that spongy-textured clinopyroxenes and spinels in Western Qinling peridotite xenoliths developed from a decompression-induced partial melting event prior to formation of melt pockets and xenolith entrainment in host magmas.

Keywords Decompression · Mantle peridotite · Partial melting · Spongy texture · Western Qinling

Introduction

Spongy textures are often found in mantle xenolith minerals such as clinopyroxene, spinel, olivine, and orthopyroxene (Andersen et al. 1984; Griffin et al. 1984; Fan and Hooper 1989; Ionov et al. 1995; Qi et al. 1995; Carpenter et al. 2002; Coltorti et al. 2004; Shaw et al. 2006; Shaw and Dingwell 2008; Dantas et al. 2009) and in mineral phenocrysts (e.g., magnetite and plagioclase) from volcanic rocks (Tsuchiyama 1985; Nelson and Montana 1992; Wark and Stimac 1992; Hibbard and Sjoberg 1994; Tepley et al. 1999; Heaman and LeCheminant 2000; Streck 2008). The spongy domains occur as porous or sieve-like rims or coronae on “nonspongy” host grains and rarely as cross-cutting veinlets, and are frequently associated with glass patches (Franz and Wirth 1997; Carpenter et al. 2002; Bonadiman et al. 2008); they have been described as “sieved texture” in some reports (Larsen 1982; Nelson and Montana 1992; Kepezhinskas et al. 1995, 1996; Shaw 2004; Shaw et al. 2006; Shaw and Dingwell 2008). Various explanations for their possible origin have been proposed on the basis of mineralogical observations, geochemical datasets, and experimental results. Many authors have

Communicated by G. Moore.

B.-X. Su (✉) · H.-F. Zhang · Y.-H. Yang · J.-F. Ying ·
Y.-J. Tang · Y. Xiao · X.-M. Zhao · Q. Mao · Y.-G. Ma
State Key Laboratory of Lithospheric Evolution, Institute of
Geology and Geophysics, Chinese Academy of Sciences, P.O.
Box 9825, Beijing 100029, China
e-mail: subenxun@mail.igcas.ac.cn

B.-X. Su · K.-Z. Qin
Key Laboratory of Mineral Resources, Institute of Geology and
Geophysics, Chinese Academy of Sciences, P.O. Box 9825,
Beijing 100029, China

B.-X. Su
Graduate University of Chinese Academy of Sciences, Beijing
100049, China

P. A. Sakyi
Department of Earth Science, University of Ghana, P.O. Box LG
58, Legon-Accra, Ghana

attributed the spongy textures to interaction of xenolith with host magma during transport (e.g., Brearley et al. 1984; Qi et al. 1995; Shaw and Klügel 2002; Shaw et al. 2006) or with exotic melts prior to entrainment, which represents a type of mantle metasomatism (e.g., Liang and Elthon 1990; Siena and Coltorti 1993; Franz and Wirth 1997; Coltorti et al. 1999; Bonadiman et al. 2008; Ionov et al. 1995, 2005). Other authors also attribute the spongy textures to incongruent partial melting induced by fluid penetration (e.g., Ionov et al. 1995; Carpenter et al. 2002; Guzmics et al. 2008) or to mineral breakdown induced by decompression (e.g., Stormer 1972; Carswell 1975; Nelson and Montana 1992).

The spongy textures in clinopyroxenes and spinels from the Western Qinling (central China) have been reported by Shi et al. (2003) and Su et al. (2007, 2009, 2010a), but little attention was paid to their origin. In the present study, we report results of a detailed petrographical, electron microprobe, and laser-ablation inductively coupled plasma mass spectrometry (LA-ICPMS) study of spongy-textured clinopyroxenes and spinels in a suite of mantle xenoliths from the Western Qinling, with the aim of placing constraints on the origin of the spongy textures.

Geological setting and sample descriptions

The Western Qinling is located in central China and is subordinate to the Kunlun–Qilian–Qinling–Dabie Mountains, a central orogenic belt in China (Zhang et al. 2001, 2002). The Cenozoic volcanic rocks in the Western Qinling (7.1–23 Ma) are sparsely distributed in the Tianshui–Lixian fault basin, which is related to extensional tectonics, and are mainly comprised of Haoti and Baiguan occurrences of kamafugites and carbonatites (Yu et al. 2003, 2004; Su et al. 2006, 2009, 2010a; Dong et al. 2008). A suite of 12 mantle xenoliths were collected from the Haoti kamafugite location for this study.

Among the studied xenoliths, 11 samples are type 1, according to previous classification [type 1, olivine forsterite content (Fo) > 90; type 2, $Fo \leq 90$; Su et al. 2009]. These samples include four garnet lherzolites, one garnet wehrlite, and six spinel-bearing/free lherzolites. One, a spinel lherzolite (HT-24), is type 2. The investigated xenoliths display clearly deformed features such as elongated mineral orientation and undulose extinction or kink band. All garnets are partially decomposed and are characterized by fresh core with an outer coronal assemblage consisting of aluminous spinel, orthopyroxene, and clinopyroxene grains, and occasionally some garnet grains are completely broken down (Su et al. 2007, 2009, 2010a). There is low modal abundance (<13% by volume, Su et al. 2009) of orthopyroxenes, most of which exhibits reactive features (Su et al.

2010a). Melt pockets are observed in all samples, comprising fine-grained olivine, clinopyroxene, and/or feldspar, phlogopite, amphibole, and glass. Spongy textures occur within most clinopyroxene grains and some spinels.

Analytical methods

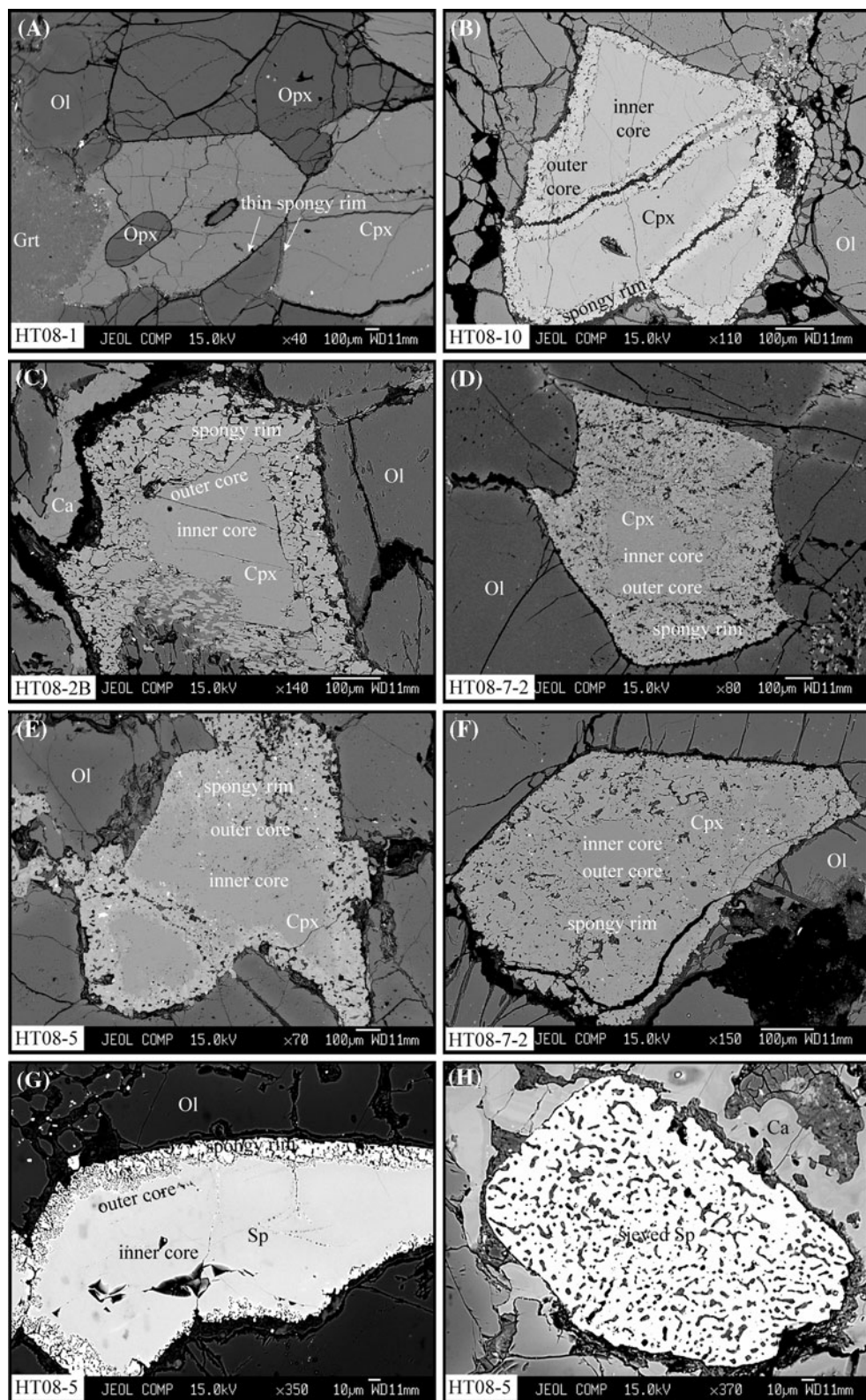
Major element compositions of minerals were obtained by wavelength-dispersive spectrometry using JEOL JXA8100 electron probe operating at accelerating voltage of 15 kV with 12 nA beam current, 5 μm beam spot, and 10–30 s counting time. The precision of all analyzed elements was better than 1.5%. Natural minerals and synthetic oxides were used as standards, and a program based on the ZAF procedure was used for data correction.

Clinopyroxenes were separated from six samples and mounted in epoxy, which was then polished to section the crystals in half for analysis. In situ trace elements were measured using laser-ablation inductively coupled plasma mass spectrometry (LA-ICPMS). Detailed analytical procedures are described elsewhere (Gao et al. 2002). Helium was used as the carrier gas to enhance transport efficiency of ablated material. The helium carrier gas inside the ablation cell was mixed with argon as a makeup gas before entering the ICP to maintain stable and optimum excitation conditions. Measurements were carried out using time-resolved analysis, operating in a fast, peak-hopping sequence in dual-detector mode. A 40 μm spot size was used in this study. Each spot analysis consisted of approximately 30 s background acquisition followed by 60 s data acquisition from the sample. Calibration was performed using NIST SRM 610 as an external calibration sample in conjunction with internal standardization using Ca. Both analyses were done at the Institute of Geology and Geophysics, Chinese Academy of Sciences. We analyzed the spongy rims in clinopyroxene grains where possible, and these results are referred to as “spongy rim + outer core” below and in illustrations.

Spongy textures of clinopyroxene and spinel

Spongy-textured clinopyroxenes and spinels mostly display nonspongy cores and spongy rims of various widths, and we refer to these features as inner core, outer core, and spongy rim, from interior to exterior. In general, the widths of the spongy rims vary from several microns to 300 μm , and clinopyroxenes in garnet peridotite display relatively thin spongy rims (Fig. 1a, b) compared with those in spinel-bearing/free lherzolites, in which the spongy texture extends into the outer core and occasionally into the inner core (Figs. 1, 2).

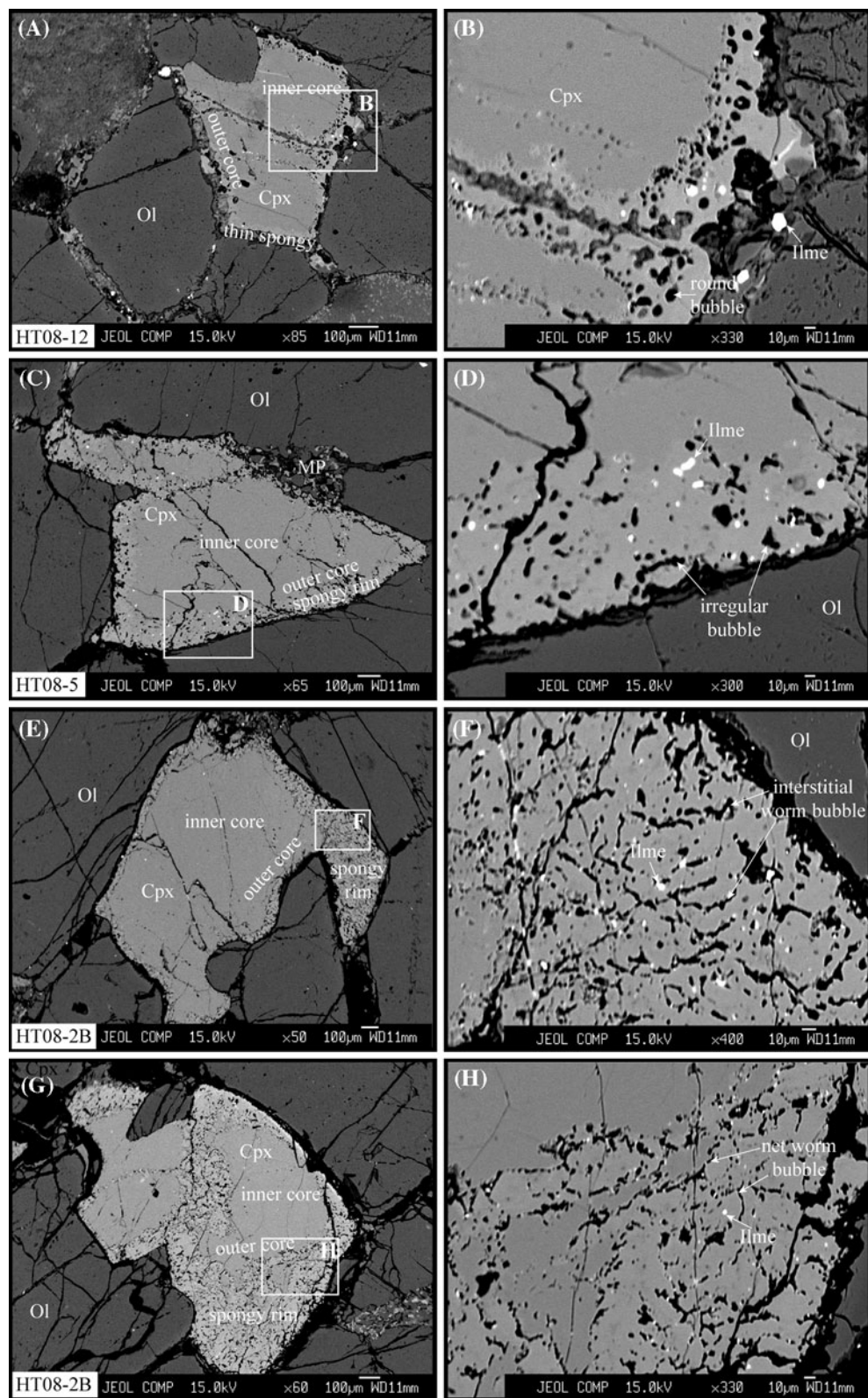
Fig. 1 Back-scattered images of spongy-textured clinopyroxenes and spinels in Western Qinling peridotite xenoliths. **a** HT08-1 garnet lherzolite: clinopyroxene with very thin spongy rim contacts with zoned olivine and breakdown garnet, and together with olivine and orthopyroxene exhibits triple junction. **b** HT08-10 garnet lherzolite: spongy rims are developed around the host clinopyroxene as well as its fractures. **c** HT08-2B garnet lherzolite: the spongy-textured clinopyroxene consists of nonspongy homogeneous core and wide spongy rim, which does not show interaction with contact carbonate vein. **d** HT08-7-2 spinel lherzolite: the clinopyroxene preserves well its primary shape and clear boundaries with contact olivines, and the spongy zone tends to develop in free space, including triple junction and wider fracture between mineral grains. **e** HT08-5 spinel lherzolite: the spongy-textured clinopyroxene is characterized by zoned core and wide-spread spongy rim, and does not show interaction with the melts, which probably reacted with zoned olivine. **f** HT08-7-2 spinel lherzolite: the relict core of the spongy-textured clinopyroxene displays zoning texture, and the spongy rim is extremely wide. **g** HT08-5 spinel lherzolite: the spongy-textured spinel consists of bright, thin spongy rim and relatively grey core. **h** HT08-5 spinel lherzolite: the sieved spinel does not show interaction with surrounding carbonate vein. *Ca* carbonate, *Cpx* clinopyroxene, *Grt* garnet, *Ol* olivine, *Opx* orthopyroxene, *Sp* spinel



Spongy-textured clinopyroxenes in garnet peridotites display well-defined boundaries between the core and the spongy rim, and these nonspongy cores do not show any

zoning pattern (Fig. 1a–c). An exception is sample HT08-1, in which olivine in contact with fragmented garnet displays a zoning pattern (Fig. 1a). However, the spongy rim of

Fig. 2 Back-scattered images of spongy-textured clinopyroxenes and their spongy rims in Western Qinling peridotite xenoliths. **a** and **b** HT08-12 garnet wehrlite: the thin spongy rim consists of relatively bright clinopyroxenes, ilmenites, and rounded bubbles. **c** and **d** HT08-5 spinel lherzolite: the bubbles and ilmenites have irregular shapes and fine grain size, respectively. **e** and **f** HT08-2B garnet lherzolite: the relatively wider spongy rim is characterized by fine-grained ilmenites and interstitial worm bubbles. **g** and **h** HT08-2B garnet lherzolite: the grain size of ilmenites becomes finer, and the worm bubbles are connected to each other. *MP* melt pocket, *Ilme* ilmenite



clinopyroxene in this sample is very limited and, therefore, could not be analyzed (Fig. 1a). The well-developed spongy-textured clinopyroxenes exhibit relatively wider

boundaries with neighboring grains (Fig. 1b, c). The spongy textures do not only develop along the rims of the grains but also occur along cracks within the grains (Fig. 1b). Some

carbonate veins around spongy-textured clinopyroxenes do not display any interactive features with the spongy rim (Fig. 1c).

Clinopyroxenes in spinel-bearing lherzolites have small cores of variable shapes and wider (100–300 µm) spongy rim (Fig. 1d–f). In back-scattered images, the cores display a zoning pattern and are slightly darker than the rims (Fig. 1e, f). The development of spongy rim depends on the space between host and ambient grains. The spongy texture tends to extend to the triple-junction point (Fig. 1d) and free space such as wider grain boundaries (Fig. 1d–f). Although spongy textures are well developed in these clinopyroxenes, the inherited shapes and primary grain boundaries are preserved (Fig. 1d, f). Some melt-like materials present around zoned olivine show no sign of interaction with the adjacent spongy-textured clinopyroxene (Fig. 1e).

Most spongy-textured spinels are characterized by large and nonspongy original cores and very thin (5–20 µm) spongy rims. The cores are homogeneous in composition and show sawlike boundaries with spongy rims (Fig. 1g). Some spinel grains are completely transformed to spongy-like structures without any relict core, and are interstitial to neighboring carbonate veins (Fig. 1h). Within these sieved spinels, worm-shaped bubbles are widespread and mostly filled with very fine (<3 µm) unknown materials and could not be analyzed by electron microprobe.

Photomicrographs of the spongy rims are shown in Fig. 2. The spongy rims consist of brighter clinopyroxene, ilmenite, and (unknown-material-filled) bubbles. The grain size of the ilmenites and the shape of the bubbles vary with the development of the spongy texture. In thin (<40 µm) spongy rims, the ilmenite grains are relatively round-shaped and coarser, ranging from 8 to 15 µm, and the bubbles are mostly round in shape (Fig. 2a, b). Wider (40–100 µm) spongy rims have irregular bubbles and ilmenite grains which are usually smaller (less than 10 µm) (Fig. 2c, d). In well-developed spongy rims (wider than 100 µm), ilmenites are much smaller in size (less than 5 µm), and worm-like bubbles (20 µm in length and 2–4 µm in width) also occur (Fig. 2e, f). The worm-like bubbles are interconnecting and the ilmenite grains become finer (<2 µm) in more developed spongy rims (Fig. 2g, h).

Mineral compositions

Major elements

Spongy-textured clinopyroxene grains are chromian diopside according to the classification of Morimoto et al. (1988; Table 1). In lherzolite, clinopyroxenes have Mg# [$Mg\# = 100 \times Mg/(Mg + Fe)$] ranging from 89.6 to 92.7,

whereas in garnet wehrlite (HT08-12), they tend to be less magnesian, with Mg# in the range of 89.2–90.3. The cores and spongy rims have very similar Mg# but differ in other major elements, particularly Na₂O, Al₂O₃, CaO, TiO₂, and FeO contents (Table 1; Fig. 3). The compositional differences from the core to the spongy rim show a consistent pattern of zoning, which is exhibited as a systematic decrease in Na₂O, Al₂O₃, and FeO, and a slight decrease in SiO₂ and MgO from core to rim, coupled with a distinct increase in CaO, TiO₂, Cr₂O₃, and Cr# [Cr# = 100 × Cr/(Cr + Al)] (Table 1; Fig. 3). The cores of clinopyroxenes displaying well-developed spongy textures show similar compositional zoning to the rims, whereas the cores of clinopyroxenes with more poorly developed spongy textures are compositionally homogeneous (Table 1).

Spongy-textured spinel shows obvious compositional variations, particularly in TiO₂, Al₂O₃, FeO, and MgO. From inner core to outer core and to spongy rim, TiO₂ increases from 0.60 wt% to 2.32 wt% and then to 4.35 wt% in the rim. Similarly, FeO increases from 13.2 wt% to 15.3 wt% up to 21.4 wt% in the rim. Conversely, Al₂O₃ and MgO, respectively, decrease from 36.2 wt% to 27.5 wt% and from 17.2 wt% to 14.4 wt%. Sieve-textured spinel has the highest contents of TiO₂ (8.02 wt%), Cr₂O₃ (34.7 wt%), and FeO (33.9 wt%), and the lowest Al₂O₃ (11.8 wt%) and MgO (8.30 wt%) contents. Accordingly, the spinel has the lowest Mg# (30.4) and highest Cr# (66.3) (Table 1).

Secondary clinopyroxenes in the melt pockets have lower Al₂O₃ (<0.30 wt%), CaO (16.4–20.0 wt%), and FeO (1.85–2.84 wt%), higher SiO₂ (53.5–56.2 wt%), Cr₂O₃ (1.50–6.00 wt%), and Na₂O (0.90–2.73 wt%), and similar TiO₂ (<0.5 wt%) contents (Su et al. 2010c) compared with the spongy-textured clinopyroxenes, and are therefore considered completely separately.

Trace elements

In the studied clinopyroxenes, although there is variation among samples, individual samples have similar normalized trace-element patterns for the core, rim, and spongy structure (Fig. 4; Table 2). The spongy rims of clinopyroxenes (except HT-24) from the type 1 xenolith display higher trace-element abundances compared with the cores. The spongy rims, especially in HT08-2B clinopyroxene, are extremely enriched in light rare-earth elements (LREE) and large-ion lithophile elements (LILE; Rb, Ba, Th, U, Sr, Pb) (Fig. 4a, b, c, d, e, f). From the core to the spongy region, there are increases in $\sum REE$, (La/Yb)_N, Nb/Ta, and Ba/Th, coupled with decreases in Y/Nb, Zr/Nb, Sm/Ba, La/Sm, and Nd/Rb and slight variations in Ti/Eu and Th/Nb (Table 2).

Clinopyroxene in HT-24 has the highest trace-element abundances (e.g., $\sum REE = 41$ –70 ppm) (Fig. 4c, d;

Table 1 In situ major element compositions of spongy-textured clinopyroxenes and spinels from Western Qinling xenoliths (cation based on six oxygens for Cpx and four for Sp)

Sample	HT08-2B GLH						HT08-4-1 LH						HT08-5 SLH						HT08-7-1 LH					
	Spongy Cpx			Spongy Cpx			Spongy Cpx			Spongy Cpx			Spongy Cpx			Spongy Cpx			Spongy Cpx					
	Mineral	Spongy	OC	IC	Spongy	OC	IC	Spongy	OC	IC	Spongy	OC	IC	Spongy	OC	IC	Spongy	OC	IC	Spongy	OC	IC		
SiO ₂	52.1	52.5	52.6	51.8	52.9	52.4	52.9	52.6	53.3	53.5	52.4	53.5	53.3	53.1	53.3	51.8	52.5	52.5	52.3					
TiO ₂	0.53	0.36	0.37	0.55	0.32	0.36	0.33	0.28	0.29	0.50	0.42	0.44	0.90	0.37	0.35	0.80	0.21	0.21	0.24					
Al ₂ O ₃	4.03	5.40	5.36	3.78	5.54	5.48	3.61	4.95	4.97	2.39	4.03	3.98	2.43	3.82	4.02	3.04	5.10	5.10	5.00					
Cr ₂ O ₃	1.35	1.39	1.36	1.57	1.38	1.46	1.68	1.50	1.47	1.26	1.13	1.25	1.27	1.07	1.15	1.16	1.40	1.40	1.32					
FeO	3.13	3.24	3.18	2.84	3.19	3.36	2.69	3.11	3.16	2.68	2.66	2.60	2.87	2.36	2.49	2.95	3.03	3.03	3.05					
MnO	0.11	0.09	0.10	0.08	0.07	0.08	0.14	0.04	0.10	0.05	0.06	0.09	0.06	0.10	0.09	0.13	0.14	0.14	0.08					
MgO	16.4	16.1	16.1	16.2	16.2	15.6	16.1	16.0	15.9	16.0	16.2	16.8	16.5	17.0	17.9	17.9	18.3	18.3						
CaO	19.6	17.6	17.6	20.9	18.1	21.1	18.5	18.5	22.5	20.3	20.6	23.6	21.9	21.8	21.8	21.8	21.8	21.8	18.7					
Na ₂ O	0.89	1.42	1.43	0.59	1.46	1.49	0.64	1.23	1.29	0.63	1.03	1.04	0.76	1.01	1.07	0.55	1.01	0.99	0.99					
Total	98.2	98.1	98.1	98.3	99.1	99.5	98.2	98.6	98.7	99.2	99.1	99.5	100.4	100.5	100.9	99.3	99.9	99.9	100.0					
Si	1.920	1.923	1.926	1.912	1.918	1.915	1.936	1.930	1.921	1.951	1.948	1.940	1.912	1.915	1.916	1.900	1.893	1.888						
Ti	0.015	0.010	0.010	0.015	0.009	0.010	0.009	0.008	0.008	0.014	0.011	0.012	0.025	0.010	0.009	0.022	0.006	0.006	0.006					
Al ^{IV}	0.080	0.077	0.074	0.088	0.082	0.085	0.064	0.070	0.079	0.049	0.052	0.060	0.088	0.085	0.084	0.100	0.107	0.107	0.112					
Al ^{VI}	0.095	0.156	0.158	0.077	0.155	0.149	0.093	0.143	0.135	0.054	0.121	0.111	0.016	0.078	0.086	0.032	0.109	0.109	0.100					
Cr	0.039	0.040	0.039	0.046	0.039	0.042	0.049	0.043	0.042	0.036	0.032	0.036	0.037	0.030	0.033	0.034	0.040	0.038						
Fe	0.096	0.099	0.097	0.088	0.097	0.102	0.083	0.095	0.096	0.082	0.081	0.079	0.088	0.071	0.075	0.090	0.091	0.092						
Mn	0.003	0.003	0.003	0.002	0.002	0.003	0.004	0.001	0.003	0.002	0.002	0.003	0.002	0.003	0.003	0.004	0.004	0.003	0.003					
Mg	0.901	0.877	0.876	0.888	0.876	0.876	0.856	0.875	0.887	0.873	0.864	0.863	0.879	0.902	0.887	0.932	0.964	0.982						
Ca	0.775	0.691	0.691	0.827	0.703	0.702	0.834	0.724	0.723	0.881	0.790	0.802	0.921	0.847	0.842	0.858	0.718	0.723						
Na	0.063	0.101	0.102	0.042	0.102	0.104	0.046	0.087	0.091	0.045	0.073	0.073	0.054	0.070	0.075	0.039	0.070	0.069						
Total	3.988	3.978	3.977	3.985	3.984	3.987	3.975	3.975	3.986	3.987	3.974	3.978	4.021	4.011	4.009	4.011	4.003	4.014						
Mg#	90.3	89.8	90.0	91.0	90.1	89.6	91.2	90.2	90.2	91.4	91.6	90.9	92.7	92.2	91.1	91.3	91.4	91.4						
Sample	HT08-7-2 SLH						HT08-9 GLH						HT08-10 GLH						HT08-11 SLH					
Mineral	Spongy Cpx			Spongy Cpx			Spongy Cpx			Spongy Cpx			Spongy Cpx			Spongy Cpx			Spongy Cpx			Spongy Cpx		
Position	Spongy	OC	IC	Spongy	OC	IC	Spongy	OC	IC	Spongy	OC	IC	Spongy	OC	IC	Spongy	OC	IC	Spongy	OC	IC	Spongy	OC	IC
SiO ₂	53.1	53.6	51.2	52.1	52.1	52.5	52.3	52.4	51.8	52.8	53.0	52.7	52.8	53.0	53.1	53.2	53.1							
TiO ₂	0.27	0.30	0.25	0.57	0.26	0.27	0.16	0.13	0.10	0.26	0.12	0.08	0.51	0.26	0.33	0.98	0.26	0.28						
Al ₂ O ₃	3.74	5.04	4.98	3.82	4.95	4.85	5.16	5.13	5.26	4.09	5.28	5.22	2.71	4.09	4.11	2.45	3.97	3.95						
Cr ₂ O ₃	1.47	2.15	1.51	1.55	1.45	1.48	1.07	1.02	1.10	1.44	1.08	1.04	1.38	1.32	1.34	1.40	1.19	1.23						
FeO	2.95	3.16	3.04	2.57	2.93	3.28	3.20	3.16	2.97	3.25	3.25	2.78	3.10	3.17	2.55	2.94	2.95							
MnO	0.13	0.12	0.11	0.11	0.14	0.06	0.11	0.09	0.06	0.11	0.10	0.11	0.11	0.11	0.11	0.10	0.03	0.11						

Table 1 continued

Sample	HT08-7-2 SLH						HT08-9 GLH						HT08-10 GLH						HT08-11 SLH								
	Spongy Cpx			Spongy Cpx			Spongy Cpx			Spongy Cpx			Spongy Cpx			Spongy Cpx			Spongy Cpx			Spongy Cpx					
	Spongy	OC	IC	Spongy	OC	IC	Spongy	OC	IC	Spongy	OC	IC	Spongy	OC	IC	Spongy	OC	IC	Spongy	OC	IC	Spongy	OC	IC			
Mineral	MgO	16.6	16.6	16.5	16.1	16.8	16.8	17.4	17.3	17.0	16.9	17.6	17.4	16.3	16.8	16.8	16.7	17.4	17.3	17.3	17.3	17.3	17.3	17.3			
Position	SiO ₂	53.8	53.2	53.3	53.7	53.3	52.8	52.4	52.5	0.08	0.08	0.01	0.33	0.16	0.07	48.6	53.0	41.6									
	TiO ₂	0.62	0.36	0.33	1.30	0.34	0.35	0.37	0.27	0.30	4.35	2.32	0.60	8.02	2.52	0.34	2.09	0.00	4.40								
	Al ₂ O ₃	0.22	5.72	5.61	0.52	5.70	5.53	1.72	3.96	3.95	27.5	28.6	36.2	11.8	18.0	29.2	3.91	0.78	9.78								
	Cr ₂ O ₃	2.24	1.25	2.25	1.19	1.17	1.42	1.25	1.21	31.2	34.1	30.1	34.7	33.3	37.1	0.58	0.06										
	FeO	3.30	3.47	3.44	2.94	3.14	2.79	2.83	2.90	21.4	15.3	13.2	33.9	34.8	14.3	4.48	7.59	16.7									
	MnO	0.03	0.11	0.12	0.07	0.09	0.08	0.07	0.11	0.11	0.22	0.27	0.18	0.39	0.53	0.24	0.04	0.05	0.17								
Total	Mg#	98.7	99.8	99.6	98.5	100.9	100.5	98.7	99.4	99.5	99.1	97.1	97.5	97.8	98.9	98.6	98.7	100.0	K ₂ O	3.14							
Mineral	Si	1.992	1.917	1.924	1.987	1.904	1.900	1.937	1.908	1.911	0.002	0.000	0.011	0.005	0.002	1.832	1.980	P ₂ O ₅	0.98								
Position	Ti	0.017	0.010	0.009	0.036	0.009	0.010	0.007	0.008	0.099	0.053	0.013	0.208	0.064	0.008	0.059	0.000	LOT	2.01								
Sample	HT08-12 GW						HT08-3 SLH						Xenocryst						Host rock								
	Spongy Cpx			Spongy Cpx			Spongy Cpx			Spongy Sp			Sieved Sp			Cpx			Kamafugite			Bulk rock					
	Spongy	OC	IC	Spongy	OC	IC	Spongy	OC	IC	Spongy	OC	IC	Spongy	OC	IC	Rim	Core	Rim	Core	Rim	Core	Rim	Core	Bulk	rock		
Mineral	SiO ₂	53.8	53.2	53.3	53.7	53.3	52.8	52.4	52.5	0.08	0.08	0.01	0.33	0.16	0.07	48.6	53.0	41.6									
Position	TiO ₂	0.62	0.36	0.33	1.30	0.34	0.35	0.37	0.27	0.30	4.35	2.32	0.60	8.02	2.52	0.34	2.09	0.00	4.40								
	Al ₂ O ₃	0.22	5.72	5.61	0.52	5.70	5.53	1.72	3.96	3.95	27.5	28.6	36.2	11.8	18.0	29.2	3.91	0.78	9.78								
	Cr ₂ O ₃	2.24	1.25	2.25	1.19	1.17	1.42	1.25	1.21	31.2	34.1	30.1	34.7	33.3	37.1	0.58	0.06										
	FeO	3.30	3.47	3.44	2.94	3.14	2.79	2.83	2.90	21.4	15.3	13.2	33.9	34.8	14.3	4.48	7.59	16.7									
	MnO	0.03	0.11	0.12	0.07	0.09	0.08	0.07	0.11	0.11	0.22	0.27	0.18	0.39	0.53	0.24	0.04	0.05	0.17								
Total	Mg#	90.9	90.4	90.7	91.8	91.1	91.3	90.4	90.6	90.5	91.0	90.6	90.5	91.3	90.6	90.4	92.1	91.4	91.3								
Sample	HT08-12 GW						HT08-3 SLH						Xenocryst						Host rock								
	Spongy Cpx			Spongy Cpx			Spongy Cpx			Spongy Sp			Sieved Sp			Cpx			Kamafugite			Bulk rock					
	Spongy	OC	IC	Spongy	OC	IC	Spongy	OC	IC	Spongy	OC	IC	Spongy	OC	IC	Rim	Core	Rim	Core	Rim	Core	Rim	Core	Bulk	rock		
Mineral	SiO ₂	53.8	53.2	53.3	53.7	53.3	52.8	52.4	52.5	0.08	0.08	0.01	0.33	0.16	0.07	48.6	53.0	41.6									
Position	TiO ₂	0.62	0.36	0.33	1.30	0.34	0.35	0.37	0.27	0.30	4.35	2.32	0.60	8.02	2.52	0.34	2.09	0.00	4.40								
	Al ₂ O ₃	0.22	5.72	5.61	0.52	5.70	5.53	1.72	3.96	3.95	27.5	28.6	36.2	11.8	18.0	29.2	3.91	0.78	9.78								
	Cr ₂ O ₃	2.24	1.25	2.25	1.19	1.17	1.42	1.25	1.21	31.2	34.1	30.1	34.7	33.3	37.1	0.58	0.06										
	FeO	3.30	3.47	3.44	2.94	3.14	2.79	2.83	2.90	21.4	15.3	13.2	33.9	34.8	14.3	4.48	7.59	16.7									
	MnO	0.03	0.11	0.12	0.07	0.09	0.08	0.07	0.11	0.11	0.22	0.27	0.18	0.39	0.53	0.24	0.04	0.05	0.17								
Total	Mg#	98.7	99.8	99.6	98.5	100.9	100.5	98.7	99.4	99.5	99.1	97.1	97.5	97.8	98.9	98.6	98.7	100.0	K ₂ O	3.14							
Mineral	Si	1.992	1.917	1.924	1.987	1.904	1.900	1.937	1.908	1.911	0.002	0.000	0.011	0.005	0.002	1.832	1.980	P ₂ O ₅	0.98								
Position	Ti	0.017	0.010	0.009	0.036	0.009	0.010	0.007	0.008	0.099	0.053	0.013	0.208	0.064	0.008	0.059	0.000	LOT	2.01								

Table 1 continued

Mineral	HT08-12 GW						HT08-3 SLH						Xenocryst						Host rock	
	Spongy Cpx			Spongy Cpx			Spongy Cpx			Spongy Cpx			Spongy Sp			Sieved Sp			Cpx	
	Spongy	OC	IC	Spongy	OC	IC	Rim	Core	Core	Bulk	rock									
Al ^{IV}	0.008	0.083	0.076	0.013	0.096	0.100	0.063	0.092	0.089	0.982	1.019	1.240	0.479	0.713	1.028	0.168	0.020	0.020	Total 99.7	
Al ^{VI}	0.002	0.160	0.163	0.010	0.144	0.134	0.011	0.078	0.081								0.005	0.005	0.015	
Cr	0.066	0.036	0.036	0.066	0.034	0.033	0.041	0.036	0.035	0.747	0.817	0.690	0.943	0.884	0.877	0.017	0.017	0.002		
Fe	0.102	0.105	0.104	0.091	0.094	0.096	0.086	0.086	0.088	0.544	0.386	0.321	0.975	0.979	0.358	0.141	0.141	0.237		
Mn	0.001	0.003	0.004	0.002	0.003	0.002	0.002	0.003	0.003	0.006	0.007	0.004	0.011	0.015	0.006	0.001	0.001	0.002		
Mg	0.856	0.865	0.872	0.834	0.877	0.882	0.925	0.936	0.922	0.649	0.736	0.746	0.426	0.471	0.759	0.783	0.783	0.721		
Ca	0.864	0.696	0.688	0.866	0.730	0.738	0.898	0.803	0.809	0.001	0.001	0.000	0.008	0.002	0.000	0.989	0.989	0.109		
Na	0.087	0.113	0.105	0.052	0.115	0.123	0.035	0.059	0.062	0.000	0.001	0.001	0.009	0.001	0.000	0.000	0.000	0.034	0.013	
Total	3.994	3.988	3.980	3.957	4.006	4.017	4.010	4.009	4.008	3.030	3.023	3.016	3.071	3.133	3.038	4.031	4.008			
Mg#	89.3	89.2	89.4	90.2	90.3	90.2	91.5	91.6	91.3	54.4	65.6	69.9	30.4	32.5	67.9	84.7	84.7	75.3		
C#										43.2	44.5	35.8	66.3	55.4	46.0					

GLH garnet lherzolite, Lh lherzolite, SLH spinel lherzolite, GW garnet wehrlite, OC inner core, IC outer core; Mg# = 100 × Mg/(Mg + Fe); Cr# = 100 × Cr/(Cr + Al). Bulk composition of kamafrige is from Dong et al. (2008)

Table 2). In contrast to other spongy-textured clinopyroxenes, the spongy rim in HT-24 clinopyroxene exhibits lower trace-element abundances than the core (Fig. 4c, d). Th, U, Nb, Ta, and Pb are more depleted in the spongy rim (Fig. 4d), and corresponding trace-element ratios have very limited variation (Table 2).

The origin of spongy textures in clinopyroxenes and spinels

General significance of spongy textures in upper mantle

Mantle metasomatism and partial melting are significant processes operating in the upper mantle, and could, respectively, refertilize or deplete the lithospheric mantle (Tsuchiyama 1986; Hibbard and Sjoberg 1994; Franz and Wirth 1997; Shaw et al. 2005; Zhang 2005; Zhang et al. 2007, 2009; Bonadiman et al. 2008; Tang et al. 2008; Su et al. 2010a, b). Mantle metasomatism processes always occur as peridotite–melt/fluid interaction and are closely related to asthenosphere upwelling and dehydration of subducted slab at variable depths in the mantle (e.g., Andersen et al. 1984; Rudnick et al. 1993; Kepezhinskas et al. 1995; Downes 2001; Zhang et al. 2007, 2009). Their signatures are mainly recorded in mineral recrystallization, zoning textures, melt pockets, and particularly compositional variations in clinopyroxenes (e.g., Lloyd 1987; Coltorti et al. 1999; Shaw et al. 2005, 2006; Zheng et al. 2005; Ying et al. 2006; Su et al. 2009, 2010a).

Spongy textures are common features reported in clinopyroxene and spinel, and occasionally in olivine and orthopyroxene (e.g., Streck 2008). Most studies attribute the spongy texture to peridotite–melt interaction (e.g., Liang and Elthon 1990; Siena and Coltorti 1993; Carpenter 1996; Franz and Wirth 1997; Coltorti et al. 1999; Bonadiman et al. 2008; Ionov et al. 1995, 2005; Shaw et al. 2006). Consequently, spongy-textured minerals could be excellent materials to understand the detailed interaction process between peridotite and melt, since they preserve reacted spongy rims and unreacted cores. On the other hand, partial melting has been suggested to be responsible for the formation of harzburgite and dunite from clinopyroxene-rich lherzolite, and its driving mechanism and imprints have been documented by many studies (e.g., Tsuchiyama 1986; Johnson et al. 1990; Chazot et al. 1994; Seyler and Bonatti 1997; Morgan and Morgan 1999; Laurora et al. 2001; Dawson 2002; Xu et al. 2003; Dasgupta and Hirschmann 2006; Stracke and Bourdon 2009). On the basis of experimental studies and analysis of natural samples, melting has been proposed as a process responsible for producing spongy textures (e.g., Stormer 1972; Carswell 1975; Nelson and Montana 1992; Ionov et al.

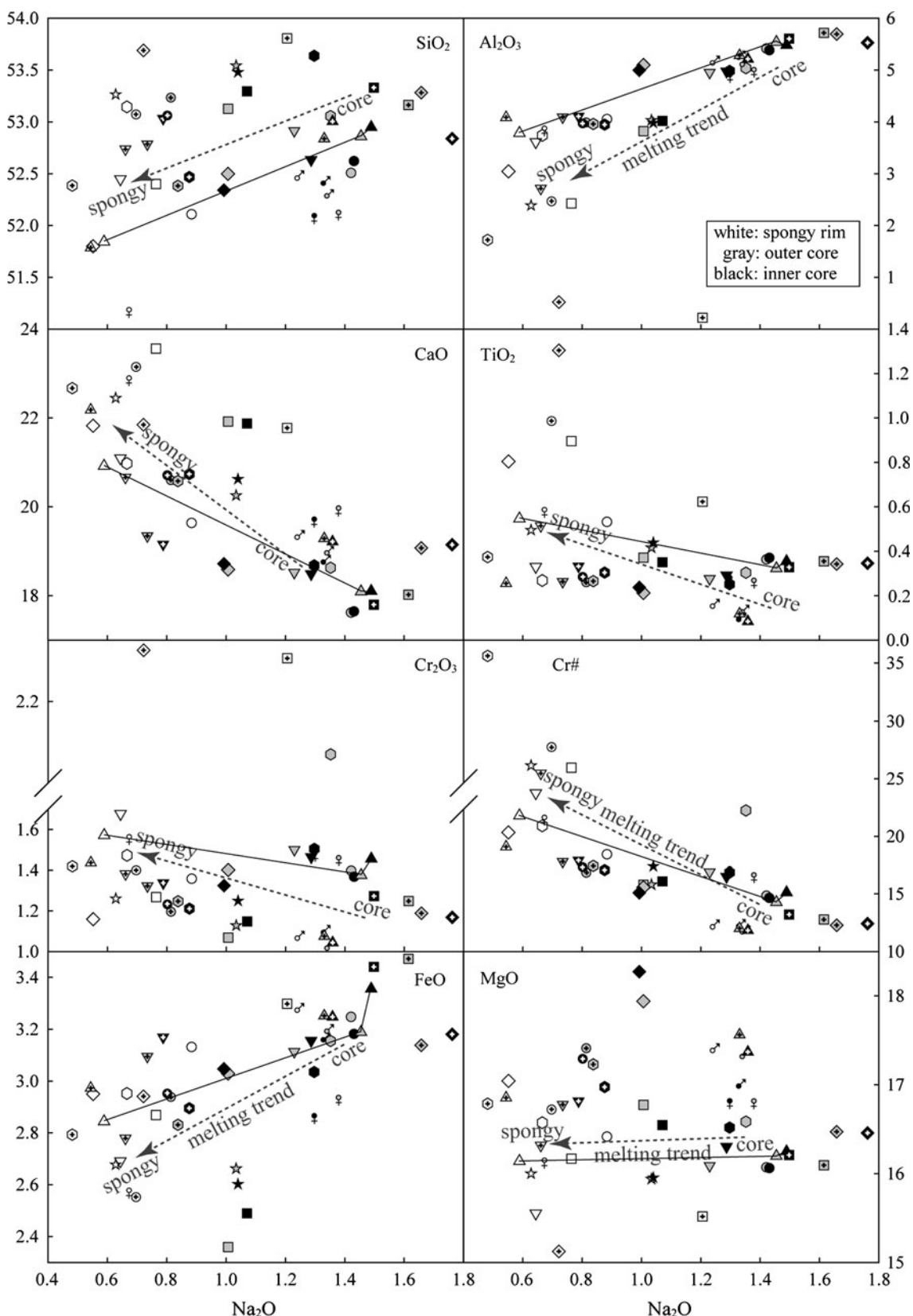


Fig. 3 Bivariate plots of spongy-textured clinopyroxenes from Western Qinling peridotite xenoliths in terms of oxides versus Na_2O (wt%). Same symbol filled with different colors represents a

single grain. Solid line connects the inner core, outer core, and spongy rim of clinopyroxene from HT08-2B as an example to show compositional variations

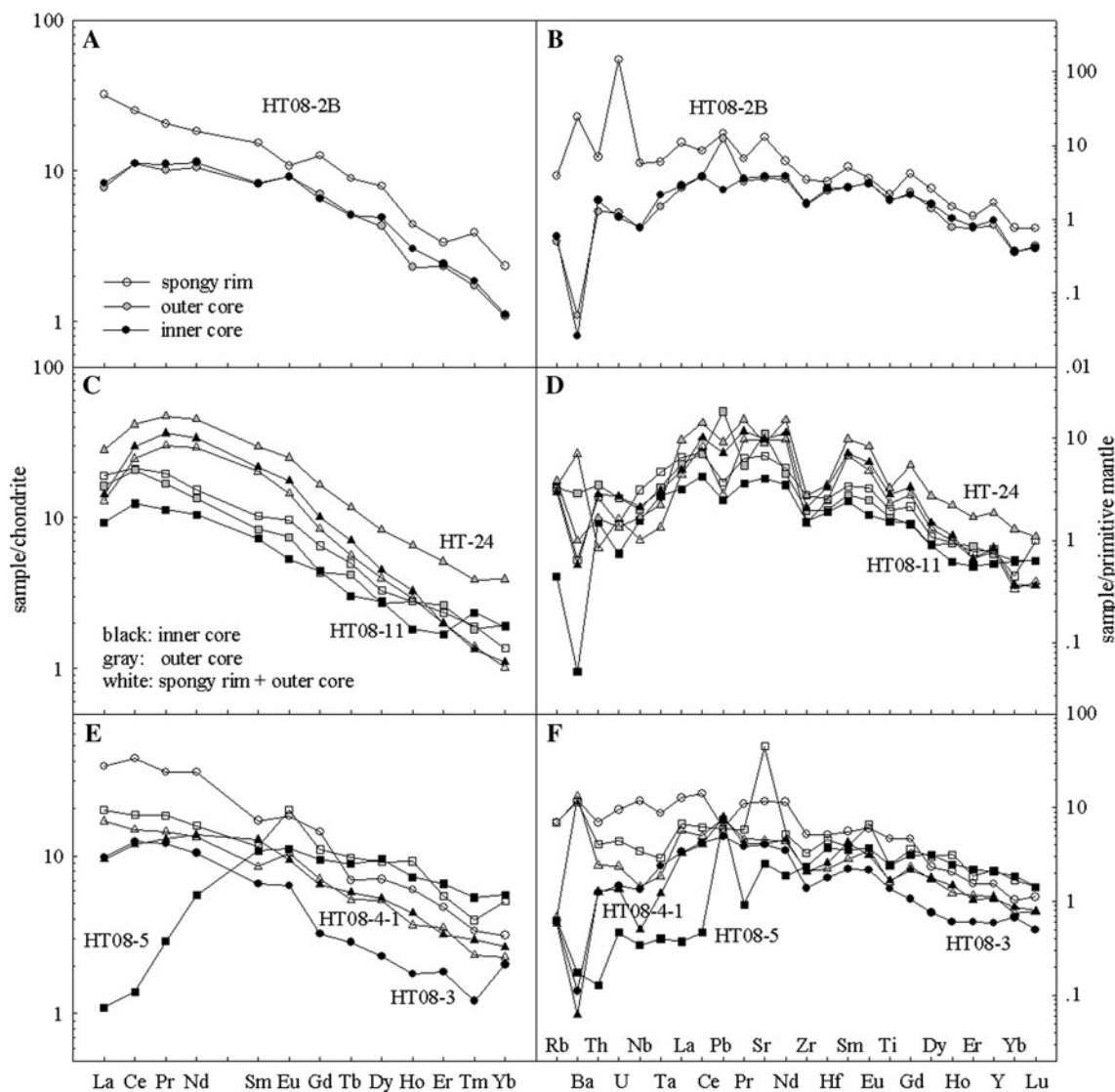


Fig. 4 Chondrite-normalized REE and primitive mantle-normalized trace-element patterns of spongy-textured clinopyroxenes from Western Qinling peridotite xenoliths. Chondrite normalizing values

are from Anders and Grevesse (1989) and primitive mantle normalizing values from Sun and McDonough 1989

1995; Carpenter et al. 2002; Guzmics et al. 2008). Consequently, the spongy texture can be used to investigate melting process and its mechanism, as well as the generation of some low-degree partial melting magmas because high-degree melting usually dissolves clinopyroxene completely.

We will discuss the origin of spongy textures, taking into account petrographical, compositional, and theoretical aspects of Western Qinling xenoliths.

Peridotite–melt interaction at mantle depth?

Assuming that peridotite–melt interaction produces the spongy texture, additional reaction features and/or relict

melt besides spongy texture should be partly left within the studied xenoliths. Zoned olivines are observed in the Western Qinling xenoliths, but their contacts with spongy-textured clinopyroxenes are poorly developed (Fig. 1a, e). Carbonate veins and spongy minerals display well-defined contacts without any apparent interaction (Figs. 1c, h and 2a). Melt pockets are good indicators for the existence of melts which might result in spongy textures. Although clinopyroxenes in contact with neighboring melt pockets exhibit spongy textures, spongy rims between their contacts have been dissolved, possibly by reaction with melts. In particular, the spongy texture along the contact between the clinopyroxene and the melt pocket has been dissolved (Fig. 5e). In contrast, the clinopyroxene spongy rims in

Table 2 In situ trace-element compositions of spongy-textured clinopyroxenes from Western Qinling xenoliths

Sample Position	HT08-2B GLH				HT08-3 SLH				HT08-4-1 LH				HT08-5 SLH				HT08-11 SLH				HT-24 SLH				
	Spongy		OC	IC	Spongy + OC		IC	Spongy + OC		IC	Spongy + OC		IC	Spongy		OC	IC	Spongy		OC	IC	Spongy		OC	IC
Li	20.0	65.7	81.7	9.80	42.1	10.2	69.1	10.3	11.0	13.4	32.9	58.8	1.97	25.8	48.9										
Sc	26.9	27.3	27.7	42.0	43.1	37.8	40.2	65.2	66.0	47.4	45.9	51.5	23.5	30.0	27.1										
Ti	2,816	2,316	2,411	6,104	1,770	2,097	2,161	3,214	3,178	2,549	2,166	1,997	2,976	4,222	3,677										
V	263	254	275	199	196	231	253	245	234	228	205	201	335	396	379										
Cr	9,854	10,326	10,752	8,162	8,800	12,486	14,056	12,057	11,155	11,794	9,794	8,754	7,906	8,259	8,276										
Mn	727	725	785	598	707	694	754	621	656	723	618	708	703	769	749										
Co	25.8	26.0	28.6	23.3	26.6	27.1	28.2	26.1	23.2	27.1	20.9	26.1	26.2	28.4	30.6										
Ni	418	510	588	387	465	540	586	433	480	450	452	421	454	430	508										
Cu	7.75	7.79	9.18	8.80	7.38	12.2	6.72	9.74	7.75	6.81	4.79	4.98	0.98	2.18	4.22										
Rb	2.47	0.32	0.37	4.48	0.38	0.43	0.37	4.45	0.40	2.09	2.06	0.28	2.19	2.45	1.89										
Sr	275	77.4	81.2	245	84.7	95.2	87.7	952	53.8	142	232	85.1	203	190	206										
Y	7.64	3.75	4.43	7.06	2.67	5.11	4.87	9.81	9.40	3.73	3.37	2.68	3.53	8.47	3.85										
Zr	38.5	17.9	18.4	58.0	15.6	23.7	23.2	36.7	26.6	30.9	21.9	17.2	16.4	30.9	23.4										
Nb	4.11	0.55	0.56	8.43	0.96	1.04	0.36	2.45	0.25	2.23	1.42	1.13	0.72	1.21	1.52										
Cs	0.13	0.13	0.13	0.10	0.12	0.11	0.11	0.30	0.10	0.11	0.06	0.08	0.09	0.21	0.07										
Ba	170	0.35	0.19	83.4	0.78	92.5	0.43	80.7	1.22	4.52	20.1	0.36	49.3	6.97	3.99										
La	7.54	1.82	1.95	875	2.31	3.90	2.25	4.60	0.26	4.48	3.82	2.19	3.04	6.61	3.35										
Ce	15.1	6.73	6.77	25.1	7.46	8.86	7.17	11.0	0.83	12.8	12.5	7.49	14.8	25.0	17.9										
Pr	1.83	0.90	0.99	3.04	1.07	1.28	1.14	1.61	0.26	1.75	1.50	1.00	2.69	4.21	3.23										
Nd	8.29	4.76	5.16	15.5	4.74	5.96	6.17	7.06	2.55	6.93	6.07	4.73	13.2	20.4	15.3										
Sm	2.26	1.20	1.22	2.47	0.98	1.26	1.88	1.70	1.59	1.51	1.23	1.07	2.98	4.36	3.18										
Eu	0.60	0.51	0.51	1.01	0.363	0.59	0.53	1.10	0.62	0.54	0.42	0.30	0.81	1.40	0.99										
Gd	2.48	1.38	1.28	2.80	0.63	1.40	1.29	2.16	1.87	1.28	0.85	0.87	1.66	3.25	1.98										
Tb	0.32	0.19	0.18	0.26	0.10	0.19	0.21	0.35	0.32	0.18	0.15	0.11	0.21	0.43	0.26										
Dy	1.92	1.05	1.19	1.73	0.56	1.27	1.31	2.23	2.32	0.80	0.66	0.68	0.96	2.02	1.10										
Ho	0.25	0.13	0.17	0.34	0.10	0.20	0.24	0.52	0.41	0.16	0.16	0.10	0.16	0.36	0.18										
Er	0.53	0.37	0.38	0.75	0.29	0.56	0.50	0.89	1.06	0.37	0.42	0.27	0.32	0.81	0.32										
Tm	0.09	0.04	0.05	0.08	0.03	0.06	0.07	0.10	0.13	0.05	0.04	0.06	0.03	0.09	0.03										
Yb	0.38	0.18	0.18	0.51	0.33	0.37	0.43	0.84	0.92	0.22	0.31	0.17	0.64	0.18											
Lu	0.06	0.03	0.08	0.04	0.06	0.06	0.11	0.11	0.07	0.05	0.05	0.03	0.08	0.03											
Hf	1.01	0.75	0.80	1.59	0.55	0.69	0.79	1.40	1.15	0.79	0.61	0.59	0.75	1.09	1.03										
Ta	0.25	0.06	0.09	0.36	0.10	0.08	0.05	0.12	0.02	0.19	0.14	0.11	0.06	0.09	0.13										
Pb	1.04	0.89	0.18	0.43	0.35	0.55	0.56	0.42	0.53	0.26	1.30	0.18	0.20	0.66	0.51										
Th	0.59	0.11	0.15	0.59	0.11	0.21	0.11	0.35	0.01	0.22	0.30	0.13	0.07	0.14	0.24										

Table 2 continued

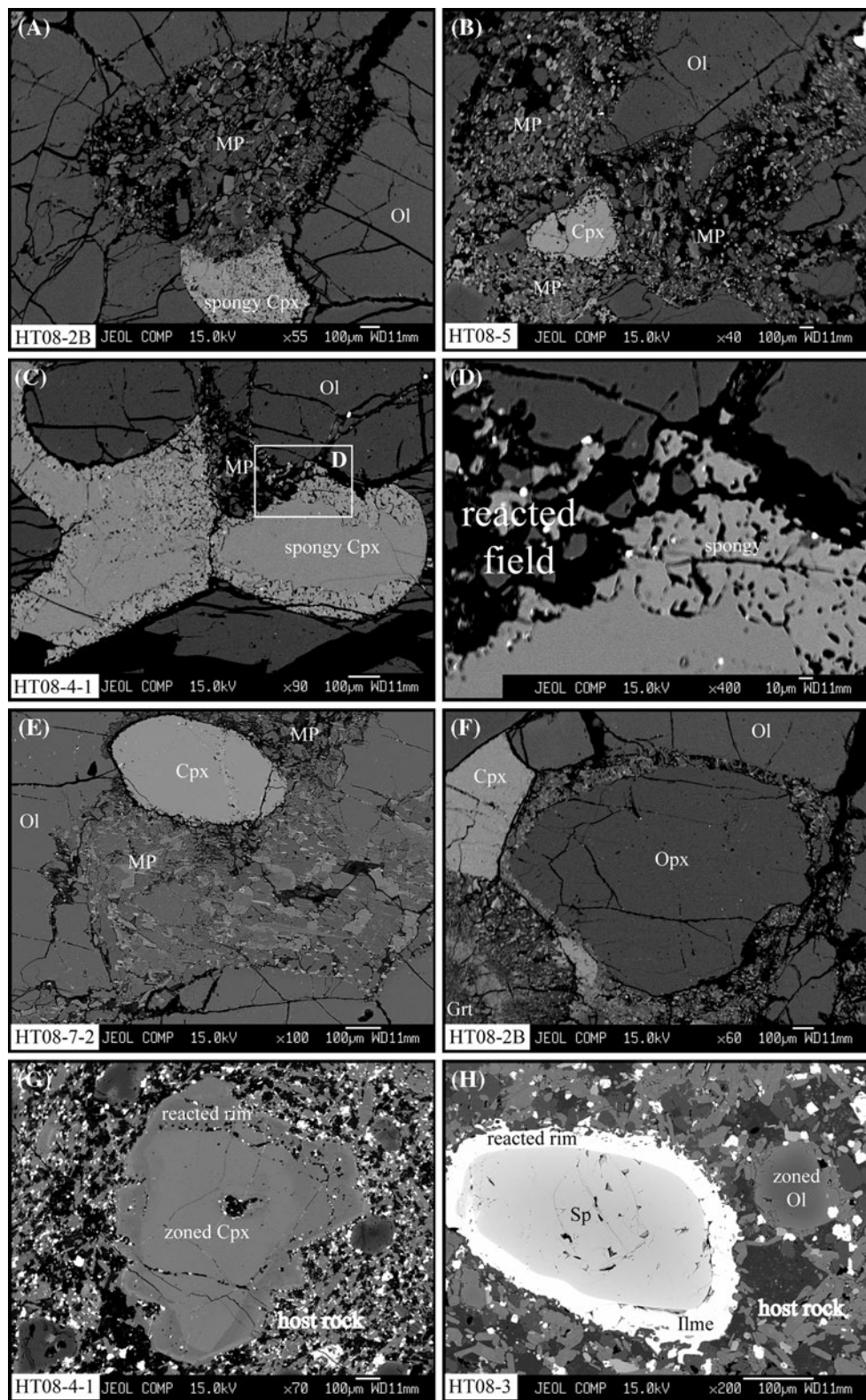
Sample Position	HT08-2B GLH			HT08-3 SLH			HT08-4-1 LH			HT08-5 SLH			HT08-11 SLH			HT-24 SLH		
	Spongy	OC	IC	Spongy + OC	IC	Spongy + OC	IC	Spongy + OC	IC	Spongy	OC	IC	Spongy	OC	IC	Spongy	OC	IC
U	3.04	0.03	0.02	0.20	0.03	0.05	0.03	0.09	0.01	0.03	0.05	0.02	0.03	0.03	0.03	0.03	0.06	
Σ REE	41.7	19.3	20.1	62.4	19.0	25.9	23.3	34.3	13.2	31.1	28.2	19.2	41.1	69.7	48.0			
Ti/Eu	4,662	4,515	4,690	6,043	4,877	3,578	4,108	2,922	5,109	4,695	5,206	6,725	3,674	3,027	3,733			
$(\text{La/Yb})_{\text{N}}$	13.7	7.12	7.46	11.9	4.80	7.30	3.62	3.79	0.19	14.0	8.42	4.91	12.8	7.20	13.0			
Nb/Ta	16.8	8.98	6.33	23.5	9.83	13.6	7.21	20.6	14.8	11.6	10.4	10.1	13.1	13.2	12.0			
Ba/Th	289	3.22	1.21	141	7.37	451	3.98	234	111	20.2	67.6	2.83	695	49.6	16.6			
Th/Nb	0.14	0.20	0.27	0.07	0.11	0.20	0.30	0.14	0.04	0.10	0.21	0.11	0.10	0.12	0.16			
Y/Nb	1.86	6.87	7.95	0.84	2.77	4.94	13.6	4.00	38.4	1.67	2.37	2.38	4.90	7.03	2.54			
Zr/Nb	9.36	32.8	33.0	6.88	16.2	22.9	64.5	15.0	109	13.8	15.4	15.2	22.8	25.7	15.5			
Sm/Ba	0.01	3.43	6.59	0.03	1.26	0.01	4.37	0.02	1.30	0.33	0.06	2.97	0.06	0.62	0.80			
La/Sm	3.34	1.52	1.60	3.54	2.36	3.10	1.20	2.71	0.16	2.97	3.11	2.04	1.02	1.52	1.06			
Nd/Rb	3.36	14.9	13.9	3.45	12.5	13.9	16.7	1.59	6.38	3.32	2.95	16.9	6.02	8.34	8.07			

contact with other primary minerals are well preserved (Figs. 2c, 5a–d). Furthermore, orthopyroxene and garnet in HT08-2B display reaction features, suggesting that these minerals had previously undergone reaction with melts; however, neighboring clinopyroxene grains have no apparent spongy texture (Fig. 5f). Most spongy-textured minerals display well-preserved primary crystal shapes and clear boundaries with surrounding grains (Figs. 1, 2), which are inconsistent with the strong infiltration and destruction mechanism of melt interaction. These petrographical features suggest that the spongy textures had formed prior to the formation of melt pockets, and that the effect of peridotite–melt interaction could not have impacted significantly on the Western Qinling xenoliths.

Metasomatized melts, whether silicate or carbonatitic within the mantle, are rich in highly mobile and incompatible elements such as K, Na, and LREE, and poor in more compatible elements such as Cr, Mg, and heavy rare-earth elements (HREE). During peridotite–melt interaction, element exchanges generally lead to enrichment in Na and LREE, and depletion in Cr# and Mg#. These elements and their ratios have been defined as indicators for metasomatism (e.g., Frey and Prinz 1978; Henry and Thomas 1984; Preb et al. 1986; Kepezhinskis et al. 1995, 1996; Xu et al. 1998, 2003; Zheng et al. 2001; Ying et al. 2006; Su et al. 2010a). For example, Ti/Eu and $(\text{La/Yb})_{\text{N}}$ ratios are considered as indicators of carbonatitic metasomatism if Ti/Eu is <1,500 and $(\text{La/Yb})_{\text{N}}$ is typically >3–4, whereas they reflect silicate metasomatism with values of >1,500 and <3–4, respectively (Rudnick et al. 1993; Klemme et al. 1995). The spongy rims in the Western Qinling clinopyroxenes show extremely low (relative to the cores) Na_2O (<0.9 wt%) and high CaO (>20 wt%), TiO_2 (>0.30 wt%), Cr_2O_3 (>1.30 wt%), Cr# (>18), $(\text{La/Yb})_{\text{N}}$ (>7.30, except one rim at 3.79), and Ti/Eu (>3,000) relative to the cores (Fig. 3; Table 2). These compositional features are inconsistent with those of previous studies and could, therefore, not be ascribed to any of the metasomatic processes proposed by such studies.

Theoretically, if indeed peridotite–melt interaction had occurred, there could probably be two stages involved in the activity of melts: the development of the spongy textures, and subsequent formation of the melt pockets. Melts in melt pockets are represented by fine-grained crystals rather than quenched glass (Figs. 2c, 5a–c, e), suggesting a long duration of crystallization. Since the melt pockets commonly occur in all xenoliths, the melt volumes should be large. Therefore, the duration and melt volume for the peridotite–melt interaction were effective in completely decomposing clinopyroxene grains or gradually zoning the clinopyroxenes without producing spongy textures. In fact, spongy rims only occur in host grains, and the cores, rims, and spongy rims generally show clear boundaries and

Fig. 5 **a** HT08-2B garnet lherzolite and **b** HT08-5 spinel lherzolite: the spongy-textured clinopyroxenes set among the melt pockets show interaction between them. **c** and **d** HT08-4-1 lherzolite: the spongy rim is partly consumed by the subsequent melts forming melt pocket. **e** HT08-7-2 spinel lherzolite: the clinopyroxene set among the melt pockets does not develop spongy texture. **f** HT08-2B garnet lherzolite: garnet and orthopyroxene exhibit reaction textures, but clinopyroxene does not. **g** and **h** Clinopyroxene and spinel xenocrysts show zoning texture and ilmenite rim, respectively, suggesting interaction with the host magmas



compositional zonation (Figs. 1, 2 and 5; Table 1) and differ in composition from the secondary clinopyroxenes in the melt pockets (Fig. 3; Su et al. 2010c). Also, it seems

difficult to explain the shape and size variations of the bubbles and ilmenites with the development of spongy rims (Fig. 2).

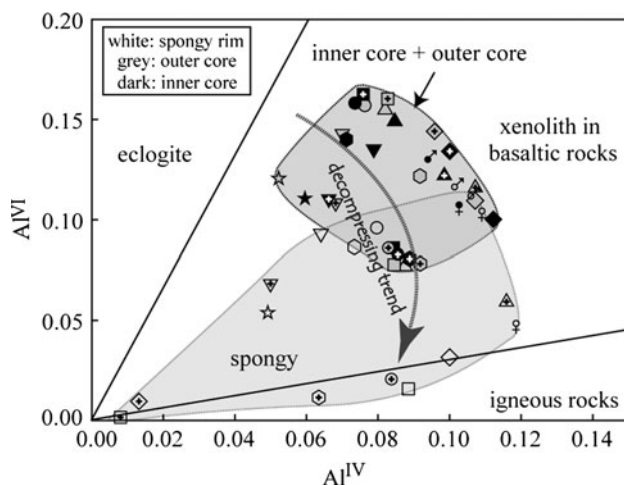


Fig. 6 Plot of Al^{IV} versus Al^{VI} of spongy-textured clinopyroxenes from Western Qinling peridotite xenoliths. The defined lines between eclogite, xenolith in basaltic rocks, and igneous rocks are from Aoki and Kushiro (1986)

Peridotite–host magma interaction during ascent?

It has been proposed that interaction with host magma during xenolith transport induces the spongy texture in mineral (e.g., Arai et al. 1994; Shaw and Klügel 2002; Shaw et al. 2006; Bonadiman et al. 2008). In the host kamacite rocks in the Western Qinling, olivine, clinopyroxene, and spinel xenocrysts were observed (Su et al. 2006; Fig. 5g, h). These xenocrysts show no spongy texture but distinct zonation (Fig. 5g, h) due to reaction with their host magmas (Su et al. 2006).

Compositionally, the host kamacites from the Western Qinling have higher Al_2O_3 (7.88–13.61 wt%), total Fe_2O_3 (10.88–13.51 wt%), and Na_2O (1.18–3.78 wt%), and lower CaO (9.54–13.35 wt%) contents (Dong et al. 2008) than the clinopyroxenes of the Western Qinling xenoliths (Table 1). Assuming that peridotite–host magma interaction occurred, the compositional differences between host magmas and clinopyroxenes could not have produced the observed compositional features, and hence the spongy textures could not have originated from interaction with the host magmas.

Partial melting induced by decompression

Hibbard and Sjoberg (1994) suggested that incongruent direct partial melting produced a spongy framework of sodian clinopyroxene and the partial melts chemically equivalent to low-sodian clinopyroxene, plagioclase, olivine, and titaniferous magnetite. The sodian clinopyroxene was transformed to low-sodian clinopyroxene by diffusional exchange of Na, Fe, and Mg (into the melt) for calcium (into the solid phase). Other studies have revealed

that spongy-textured clinopyroxene is significantly depleted in Na and Al relative to “intact” clinopyroxene, whereas the glass patches within the “spongy” clinopyroxene, in contrast, are highly enriched in these elements (e.g., Carswell 1975; Carpenter et al. 2002; Guzmics et al. 2008) as well as TiO_2 (Lee et al. 1993). The compositions of the spongy-textured clinopyroxenes from the Western Qinling are depleted in Na_2O , Al_2O_3 , and FeO , and enriched in TiO_2 (Fig. 3; Table 1). Cr# increase and Al_2O_3 content decrease have been distinguished as indicators of partial melting (Frey and Prinz 1978; Henry and Thomas 1984; Preb et al. 1986). The spongy-textured spinels in the Western Qinling xenoliths display Cr# varying from 35.8 to 43.2 and Al_2O_3 from 36.2 wt% to 27.5 wt% from the cores to the spongy rims. These features are in agreement with the results of experiments and natural sample studies mentioned above, suggesting a partial melting agent.

Partial melting might result from decreasing pressure and an increase in temperature. High-pressure piston-cylinder experiments by Nelson and Montana (1992) indicated that decompression is a simple mechanism to produce spongy texture, as it requires no addition of heat or mass. Petrographical and compositional observations of experiments and natural sample studies also suggested that decompression partial melting is responsible for the formation of spongy texture (Tsuchiyama 1986; Faure et al. 2001). The spongy-textured minerals in this study display interstitial features and clear primary contact relations with ambient grains or carbonate veins. Many clinopyroxenes consist of nonspongy cores and thin spongy rims which have no reaction signature with exotic melts including carbonate or melt pockets (Figs. 1, 2, 5). The spongy texture tends to expand its development to triple junction and wider grain boundaries (Figs. 1b–e and 2c, e, g), where space is available for decompression. Clinopyroxenes from the spinel-bearing peridotites in shallow lithospheric mantle have wider spongy rims than those from garnet peridotites at deep levels, suggesting that the decompression occurred at higher levels and that the garnet peridotites were less affected by this decompression.

Wass (1979) showed that there are compositional differences between high- and low-pressure clinopyroxenes based on trends of decreasing Al^{IV} at the expense of silica and the increase in the $\text{Al}^{\text{IV}}/\text{Al}^{\text{VI}}$ ratio, coupled with increase in TiO_2 . The $\text{Al}^{\text{IV}}/\text{Al}^{\text{VI}}$ ratio in clinopyroxene is a function of the silica activity of the melt from which it crystallizes, thus changes in this ratio may reflect pressure differences (Wass 1979; Aoki and Kushiro 1986). The Al^{IV} versus Al^{VI} diagram (Fig. 6) shows a decrease in both Al^{VI} value and $\text{Al}^{\text{IV}}/\text{Al}^{\text{VI}}$ ratio from the cores to the spongy rims, in conjunction with the high TiO_2 and low SiO_2 of the spongy rims (Table 1; Fig. 3), demonstrating a significant decompression trend. Ilmenite lamellae are usually

exsolved from clinopyroxenes during decompression (e.g., Zhang and Liou 1999; Zhang et al. 2003; Liou et al. 2007; Patel et al. 2009), which could explain the occurrence of ilmenite grains within the spongy rims.

The decompression event is probably related to the tectonic extension in the Western Qinling and the formation of the Tianshui–Lixian fault basin (Zhang et al. 2001; Yu et al. 2003, 2004, 2005; Dong et al. 2008; Su et al. 2007, 2009, 2010a), which may be why the occurrence of peridotite xenoliths in these magmas is limited to this fault basin.

However, the trace-element features, particularly the enrichment in Sr, Ba, Nb, Zr, and LREE and the depletion in Ni, could not be interpreted as decompression melting. These trace-element features were probably caused by laser analysis. As mentioned in the analytical methods section, for each analysis of the spongy part, the laser beam had a spot diameter of 40 μm . Some spongy rims in clinopyroxene grains could not be independently determined since they were smaller than the beam spot size. The spongy parts consist of different materials such as clinopyroxene, ilmenite, and (melt-filled) bubbles. The beam size appears to be too large to confidently resolve the clinopyroxene part alone. For example, electron probe analysis of the spongy rims of the HT08-2 clinopyroxenes yielded TiO_2 contents of 0.53 wt% (Ti, 3,177 ppm) and 0.55 wt% (Ti, 3,297 ppm), which are different from the laser-analyzed result of 2,816 ppm in Ti (Tables 1, 2). Therefore, the laser data is a “bulk analysis” of the spongy parts and does not represent the real compositions of the pure clinopyroxenes in the spongy rims. The above trace-element features, particularly enrichment in Sr, Ba, and LREE, may have been contributed by carbonates which occur as veins around the spongy clinopyroxenes (Fig. 1c). However, the trace-element compositions of the cores record the signatures of the primary clinopyroxenes.

Where were the partial melts going?

High-degree partial melting within the upper mantle could generate large-volume melts for magma activity. The spongy textures may reflect decompression melting. The small volume of partial melts generated in the spongy rims could not gather to generate magmas and instead remained around the host grain or migrated only very short distances away. During migration, the more active elements such as Na and Al preferentially migrate, leaving behind the less active elements such as Ca, Ti, and Cr, and the present spongy compositions depend on the extent of migration and/or retention of these elements.

The bubbles occurring in the spongy rims are likely to be the partial melt container in the earlier stages of partial melting. With the advancing development of spongy

textures, the bubble shape varies from round, irregular, interstitial, worm-like shapes to a network of bubbles (Fig. 2), suggesting a vivid scenario involving generation, gathering, and migration of partial melts. However, most bubbles are empty at present, and glass is rarely observed around spongy-textured grains. Therefore, it is difficult to infer the final gathering point of the partial melts. However, considering subsequent melt activity forming the melt pockets, we speculate that the partial melts from the spongy-textured minerals possibly provided some contributions to the formation of melt pockets.

Conclusions

Clinopyroxenes and spinels in Western Qinling peridotite xenoliths have developed spongy textures consisting of nonspongy cores and spongy rims. The spongy rims include low-Na clinopyroxene, bubbles, and ilmenites, with the latter two displaying shapes and sizes that vary with the width of the spongy texture. Compositionally, the spongy rims are enriched in Ca, Ti, Cr#, and most trace elements, and depleted in Na, Al, Fe, Al^{VI} , and $\text{Al}^{\text{IV}}/\text{Al}^{\text{VI}}$ compared with the cores. Based on petrological and chemical compositions of the minerals, we propose that the spongy-textured clinopyroxenes and spinels in the Western Qinling xenoliths developed from a decompression-induced melting event occurring under mantle conditions prior to xenolith entrainment in the host magma.

Acknowledgments This research was financially supported by the National Science Foundation of China (grants 90714008 and 40721062) and the Special Research Project (Grant 1008) of the State Key Laboratory of Lithospheric Evolution, Institute of Geology and Geophysics, Chinese Academy of Sciences. The authors would like to extend their sincere gratitude to Dr. Benny Chisonga for improving the English language and to the editor, M.J. Streck, and another anonymous reviewer for editorial handling and constructive comments.

References

- Anders E, Grevesse N (1989) Abundances of the elements: meteoritic and solar. *Geochim et Cosmochim Acta* 53:197–214
- Andersen T, O'Reilly SY, Griffin WL (1984) The trapped fluid phase in upper mantle xenoliths from Victoria, Australia: implications for mantle metasomatism. *Contrib Mineral Petrol* 88:72–85
- Aoki K, Kushiro I (1986) Some clinopyroxenes from ultramafic inclusions in Dreiser Weiher, Eifel. *Contrib Mineral Petrol* 18:326–337
- Arai S, Abe N, Ninomiya A (1994) Reaction of peridotite xenoliths with host magmas as an analogue of mantle–melt interaction: microscopic characteristics. *Sci Rep Kanazawa University* 39:65–99
- Bonadiman C, Coltorti M, Beccaluva L, Siena F (2008) Mantle metasomatism vs. host magma interaction: the ongoing controversy. *Geophysical Research Abstracts* 10, EGU2008-A-09723

- Brearley M, Scarfe CM, Fujii T (1984) The petrology of ultramafic xenoliths from Summit Lake, near Prince George, British Columbia. *Contrib Mineral Petrol* 88:53–63
- Carpenter RL (1996) Petrology of mantle xenoliths hosted in Tertiary magmas of the Hessian Depression, Germany: a comparison to xenoliths from Quaternary magmas of the West Eifel. PhD Thesis, University of Western Ontario.
- Carpenter RL, Edgar AD, Thibault Y (2002) Origin of spongy textures in clinopyroxene and spinel from mantle xenoliths, Hessian Depression, Germany. *Mineral Petrol* 74:149–162
- Carswell DA (1975) Primary and secondary phlogopites and clinopyroxenes in garnet lherzolite xenoliths. *Phys Chem Earth* 9:417–429
- Chazot G, Menzies MA, Harte B, Matthey D (1994) Carbonatite metasomatism and melting of the Arabian lithosphere: evidence from oxygen isotopes and trace element composition of spinel lherzolites. *Mineral Mag* 58A:167–168
- Coltorti M, Bonadiman C, Hinton RW, Siena F, Upton BG (1999) Carbonatite metasomatism of the ocean upper mantle: evidence from clinopyroxenes and glasses in ultra-mafic xenoliths of Grande Comore, Indian Ocean. *J Petrol* 40:133–165
- Coltorti M, Beccaluva L, Bonadiman C, Faccini B, Ntaflos T, Siena F (2004) Amphibole genesis via metasomatic reaction with clinopyroxene in mantle xenoliths from Victoria Land, Antarctica. *Lithos* 75:115–139
- Dantas C, Grégoire M, Koeste E, Conceição RV, Rieck N (2009) The lherzolite-websterite xenolith suite from Northern Patagonia (Argentina): evidence of mantle–melt reaction processes. *Lithos* 107:107–120
- Dasgupta R, Hirschmann MM (2006) Melting in the Earth's deep upper mantle caused by carbon dioxide. *Nature* 440:659–662
- Dawson JB (2002) Metasomatism and partial melting in upper-mantle peridotite xenoliths from the Lashaine volcano, Northern Tanzania. *J Petrol* 43:1749–1777
- Dong X, Zhao ZD, Mo XX, Yu XH, Zhang HF, Li B, Depaolo DJ (2008) Geochemistry of the Cenozoic kamafugites from west Qinling and its constraint for the nature of magma source region. *Acta Petrologica Sinica* 24:238–248 (in Chinese with English abstract)
- Downes H (2001) Formation and modification of the shallow sub-continental lithospheric mantle: a review of geochemical evidence from ultramafic xenolith suites and tectonically emplaced ultramafic massifs of western and central Europe. *J Petrol* 42:233–250
- Fan QC, Hooper PR (1989) The mineral chemistry of ultramafic xenoliths of eastern China: implications for upper mantle composition and the paleogeotherms. *J Petrol* 30:1117–1158
- Faure F, Trolliard G, Montel JM, Nicollet C (2001) Nano-petrographic investigation of a mafic xenolith (Maar de Beaunit, Massif Central, France). *Eur J Mineral* 13:27–40
- Franz L, Wirth R (1997) Thin intergranular melt films and melt pockets in spinel peridotite xenoliths from the Rhon area (Germany): early stage of melt generation by grain boundary melting. *Contrib Mineral Petrol* 129:268–283
- Frey FA, Prinz M (1978) Ultramafic inclusions from San Carlos, Arizona: petrologic and geochemical data bearing on their petrogenesis. *Earth Planet Sci Lett* 38:129–176
- Gao S, Liu X, Yuan H, Hattendorf B, Günther D, Chen L, Hu S (2002) Analysis of forty-two major and trace elements of USGS and NIST SRM glasses by LA-ICPMS. *Geostand Geoanal Res* 26:181–196
- Griffin WL, Wass SY, Hollis JD (1984) Ultramafic xenoliths from Bullenmerri and Gnotuk Maars, Victoria, Australia: petrology of a sub-continental crust-mantle transition. *J Petrol* 25:53–87
- Guzmics T, Kodolányi J, Kovács I, Szabó C, Bali E, Ntaflos T (2008) Primary carbonatite melt inclusions in apatite and in K-feldspar of clinopyroxene-rich mantle xenoliths hosted in lamprophyre dikes (Hungary). *Mineral Petrol* 94:225–242
- Heaman LM, LeCheminant AN (2000) Anomalous U-Pb systematic in mantle-derived baddeleyite xenocrysts from Ille Bizard: evidence for high temperature radon diffusion? *Chem Geol* 172:77–93
- Henry JBD, Thomas B (1984) Chromian spinel as a petrogenetic indicator in abyssal and alpine-type peridotites and spatially associated lavas. *Contrib Mineral Petrol* 86:54–76
- Hibbard MJ, Sjoberg JJ (1994) Signs of incongruent melting of clinopyroxene in Limbergite, Thetford hill, Vermont. *Can Mineral* 32:307–317
- Ionov DA, Prikhod'ko VS, O'Reilly SY (1995) Peridotite xenoliths in alkali basalts from the Sikhote-Alin southeastern Siberia, Russia: trace-element signatures of mantle beneath a convergent continental margin. *Chem Geol* 120:275–294
- Ionov DA, Chanefo I, Bodinier JL (2005) Origin of Fe-rich lherzolites and wehrlites from Tok, SE Siberia by reactive melt percolation in refractory mantle peridotites. *Contrib Mineral Petrol* 150:335–353
- Johnson KTM, Dick HJB, Shimizu N (1990) Melting in the oceanic upper mantle: an ion microprobe study of diopsides in abyssal peridotites. *J Geophys Res* 95:2661–2678
- Kepezhinskas P, Defant MJ, Drummond MS (1995) Na metasomatism in the island-arc mantle by slab melt–peridotite interaction: evidence from mantle xenoliths in the north Kamchatka arc. *J Petrol* 36:1505–1527
- Kepezhinskas P, Defant MJ, Drummond MS (1996) Progressive enrichment of island arc mantle by melt–peridotite interaction inferred from Kamchatka xenoliths. *Geochim Cosmochim Acta* 60:1217–1229
- Klemme S, van der Laan SR, Foley SF, Gunther D (1995) Experimentally determined trace and minor element partitioning between clinopyroxene and carbonatite melt under upper mantle conditions. *Earth Planet Sci Lett* 133:439–448
- Larsen JG (1982) Mantle-derived dunite and lherzolite nodules from Ubekendt Ejland, west Greenland Tertiary province. *Mineral Mag* 46:329–336
- Laurora A, Mazzucchelli M, Rivalenti G, Vannucci R (2001) Metasomatism and melting in carbonated peridotite xenoliths from the mantle wedge: the Gobernador Gregores case (Southern Patagonia). *J Petrol* 42:69–87
- Lee DC, Halliday AN, Hunter RH, Holden P, Upton BGJ (1993) Rb-Sr and Sm-Nd isotopic variations in dissected crustal xenoliths. *Geochim Cosmochim Acta* 57:219–230
- Liang Y, Elthon D (1990) Geochemistry and petrology of spinel lherzolite xenoliths from Xalapasco de La Joya, San Luis Potosí, Mexico: partial melting and mantle metasomatism. *J Geophys Res* B95:15859–15877
- Liou JG, Zhang RY, Ernst WG (2007) Very high-pressure orogenic garnet peridotites. *Proc Nat Acad Sci* 104:9116–9121
- Lloyd FE (1987) Characterization of mantle metasomatic fluids in spinel lherzolite and alkali clinopyroxenites from the West Eifel and Uganda. In: Menzies MA, Hawkesworth CJ (eds) Mantle metasomatism. Academic, London, pp 91–123
- Morgan JP, Morgan WJ (1999) Two-stage melting and the geochemical evolution of the mantle: a recipe for mantle plum-pudding. *Earth Planet Sci Lett* 170:215–239
- Morimoto N, Fabries J, Ferguson AK, Ginzburg IV, Ross M, Seifert FA, Zussman J, Aoki K, Gottardi G (1988) Nomenclature of pyroxenes. *Am Mineral* 73:1123–1133
- Nelson ST, Montana A (1992) Sieve-textured plagioclase in volcanic rocks produced by rapid decompression. *Am Mineral* 77:1242–1249
- Patel SC, Ravi S, Anilkumar Y, Naik A, Thakur SS, Pati JK, Nayak SS (2009) Mafic xenoliths in Proterozoic kimberlites from

- Eastern Dharwar Craton, India: mineralogy and P-T regime. *J Asian Earth Sci* 34:336–346
- Preb S, Witt G, Seck HA, Eonov D, Kovalenko VI (1986) Spinel peridotite xenoliths from the Tariat Depression, Mongolia: major element chemistry and mineralogy of a primitive mantle xenolith suite. *Geochim Cosmochim Acta* 50:2587–2599
- Qi Q, Taylor LA, Zhou XM (1995) Petrology and geochemistry of mantle peridotite xenoliths from SE China. *J Petrol* 36:55–79
- Rudnick LR, McDonough WF, Chappell BW (1993) Carbonatite metasomatism in the northern Tanzanian mantle: petrographic and geochemical characteristics. *Earth Planet Sci Lett* 114:463–475
- Seyler M, Bonatti E (1997) Regional-scale melt-rock interaction in lherzolitic mantle in the Romanche Fracture Zone (Atlantic Ocean). *Earth Planet Sci Lett* 146:273–287
- Shaw CSJ (2004) The temporal evolution of three magmatic systems in the West Eifel volcanic field, Germany. *J Volcanol Geotherm Res* 131:213–240
- Shaw CSJ, Dingwell DB (2008) Experimental peridotite–melt reaction at one atmosphere: a textural and chemical study. *Contrib Mineral Petrol* 155:199–214
- Shaw CSJ, Klügel A (2002) The pressure and temperature conditions and timing of glass formation in mantle-derived xenoliths from Baarley West Eifel, Germany: the case for amphibole breakdown, lava infiltration and mineral–melt reaction. *Mineral Petrol* 74:163–187
- Shaw CSJ, Eyzaguirre J, Fryer B, Gagnon J (2005) Regional variations in the mineralogy of metasomatic assemblages in mantle xenoliths from the West Eifel volcanic field, Germany. *J Petrol* 46:945–972
- Shaw CSJ, Heidelbach F, Dingwell DB (2006) The origin of reaction textures in mantle peridotite xenoliths from Sal Island, Cape Verde: the case for “metasomatism” by the host lava. *Contrib Mineral Petrol* 151:681–697
- Shi LB, Lin CY, Chen XD (2003) Composition, thermal structures and rheology of the upper mantle inferred from mantle xenoliths from Haoti, Dangchang, Gansu Province, western China. *Seismol Geol* 4:525–542 (in Chinese with English abstract)
- Siena F, Coltorti M (1993) Thermobarometric evolution and metasomatic processes of upper mantle in different tectonic settings: evidence from spinel peridotite xenoliths. *Eur J Mineral* 5:1073–1090
- Stormer JC (1972) Mineralogy and petrology of the Raton-Clayton volcanic field, northeastern New Mexico. *Geol Soc Am Bull* 83:3299–3322
- Stracke A, Bourdon B (2009) The importance of melt extraction for tracing mantle heterogeneity. *Geochim Cosmochim Acta* 73:218–238
- Streck MJ (2008) Mineral textures and zoning as evidence for open system processes. *Rev Mineral Geochem* 69:595–622
- Su BX, Zhang HF, Xiao Y, Zhao XM (2006) Characteristics and geological significance of olivine xenocrysts in Cenozoic volcanic rocks from western Qinling. *Prog Nat Sci* 16:1300–1306
- Su BX, Zhang HF, Wang QY, Sun H, Xiao Y, Ying JF (2007) Spinel-garnet phase transition zone of Cenozoic lithospheric mantle beneath the eastern China and western Qinling and its T-P conditions. *Acta Petrologica Sinica* 23:1313–1320 (in Chinese with English abstract)
- Su BX, Zhang HF, Ying JF, Xiao Y, Zhao XM (2009) Nature and processes of the lithospheric mantle beneath the western Qinling: evidence from deformed peridotitic xenoliths in Cenozoic kamacites from Haoti, Gansu Province, China. *J Asian Earth Sci* 34:258–274
- Su BX, Zhang HF, Saky PA, Ying JF, Tang YJ, Yang YH, Qin KZ, Xiao Y, Zhao XM (2010a) Compositionally stratified lithosphere and carbonatite metasomatism recorded in mantle xenoliths from the Western Qinling (Central China). *Lithos* 116:111–128
- Su BX, Zhang HF, Tang YJ, Chisong B, Qin KZ, Ying JF, Sayki PA (2010b) Geochemical syntheses among the cratonic, off-cratonic and orogenic garnet peridotites and their tectonic implications. *Int J Earth Sci.* doi: [10.1007/s00531-010-0527-0](https://doi.org/10.1007/s00531-010-0527-0)
- Su BX, Zhang HF, Saky PA, Qin KZ, Ying JF, Tang YJ, Liu PP, Xiao Y, Zhao XM, Mao Q, Ma YG (2010c) Formation of melt pockets in mantle peridotite xenoliths from the Western Qinling (Central China): partial melting and metasomatism. *J Earth Sci* (in press)
- Sun SS, McDonough WF (1989) Chemical and isotopic systematic of oceanic basalt: implication for mantle composition and processes. In: Saunders AD, Norry MJ (Eds.) *Magmatism in the oceanic basins*, Special Publication of Geological Society of London, vol 42, pp 313–346
- Tang YJ, Zhang HF, Ying JF, Zhang J, Liu XM (2008) Refertilization of ancient lithospheric mantle beneath the central North China Craton: evidence from petrology and geochemistry of peridotite xenoliths. *Lithos* 101:435–452
- Tepley FJ, Davidson JP, Clyne MA (1999) Magmatic interactions as recorded in plagioclase phenocrysts of Chaos Crags, Lassen Volcanic Center, California. *J Petrol* 40:787–806
- Tsuchiyama A (1985) Dissolution kinetics of plagioclase in the melt of the system diopside-albite-anorthite, and origin of dusty plagioclase in andesites. *Contrib Mineral Petrol* 89:1–16
- Tsuchiyama A (1986) Melting and dissolution kinetics: application to partial melting and dissolution of xenoliths. *J Geophys Res* 91:9395–9406
- Wark DA, Stimac JA (1992) Origin of mantled (rapakivi) feldspars: experimental evidence of a dissolution- and diffusion-controlled mechanism. *Contrib Mineral Petrol* 111:345–361
- Wass S (1979) Multiple origins of clinopyroxenes in alkali basaltic rocks. *Lithos* 12:115–132
- Xu YG, Menzies MA, Vroon P, Mercier JC, Lin CY (1998) Texture–temperature–geochemistry relationships in the upper mantle as revealed from spinel peridotite xenoliths from Wangqing, NE China. *J Petrol* 39:469–493
- Xu YG, Menzies MA, Thirlwall MF, Huang XL, Liu Y, Chen XM (2003) “Reactive” harzburgites from Huinan, NE China: products of the lithosphere–asthenosphere interaction during lithospheric thinning? *Geochim Cosmochim Acta* 67:487–505
- Ying JF, Zhang HF, Kita N, Morishita Y, Shimoda G (2006) Nature and evolution of Late Cretaceous lithospheric mantle beneath the eastern North China craton: constraints from petrology and geochemistry of peridotitic xenoliths from Junan, Shandong Province, China. *Earth Planet Sci Lett* 244:622–638
- Yu XH, Mo XX, Su SG, Dong FL, Zhao X, Wang C (2003) Discovery and significance of Cenozoic volcanic carbonatite in Lixian, Gansu Province. *Acta Petrologica Sinica* 19:105–112 (in Chinese with English abstract)
- Yu XH, Zhao ZD, Mo XX, Wang YL, Xiao Z, Zhu DQ (2004) Trace element, REE and Sr, Nd, Pb isotopic geochemistry of Cenozoic kamacites and carbonatite from west Qinling, Gansu Province: implication of plume–lithosphere interaction. *Acta Petrologica Sinica* 20:483–494 (in Chinese with English abstract)
- Yu XH, Zhao ZD, Mo XX, Zhou S, Zhu DQ, Wang YL (2005) $^{40}\text{Ar}/^{39}\text{Ar}$ dating for Cenozoic kamacites from western Qinling in Gansu Province. *Chin Sci Bull* 50:2638–2643
- Zhang HF (2005) Transformation of lithospheric mantle through peridotite–melt reaction: a case of Sino-Korean craton. *Earth Planet Sci Lett* 237:768–780
- Zhang RY, Liou JG (1999) Exsolution lamellae in minerals from ultrahigh-P rocks. *Int Geol Rev* 41:981–993
- Zhang GW, Zhang BR, Yuan XC, Xiao Q (2001) Qinling orogenic belt and continental dynamics. Science Press, Beijing, pp 1–855 (in Chinese)

- Zhang GW, Dong YP, Yao AP (2002) Some thoughts on study of continental dynamics and orogenic belt. *Geol China* 29:7–13 (in Chinese with English abstract)
- Zhang RY, Zhai SM, Fei YW, Liou JG (2003) Titanium solubility in coexisting garnet and clinopyroxene at very high pressure: the significance of exsolved rutile in garnet. *Earth Planet Sci Lett* 216:591–601
- Zhang HF, Nakamura E, Kobayashi K, Zhang J, Ying JF, Tang YJ, Niu LF (2007) Transformation of subcontinental lithospheric mantle through peridotite-melt reaction: evidence from a highly fertile mantle xenolith from the North China craton. *Int Geol Rev* 49:658–679
- Zhang HF, Goldstein SL, Zhou XH, Sun M, Cai Y (2009) Comprehensive refertilization of lithospheric mantle beneath the North China Craton: further Os-Sr-Nd isotopic constraints. *J Geol Soc* 166:249–259
- Zheng JP, O'Reilly SY, Griffin WL, Lu FX, Zhang M, Pearson NJ (2001) Relics of refractory mantle beneath the eastern North China block: significance for lithosphere evolution. *Lithos* 57:43–66
- Zheng JP, Zhang RY, Griffin WL, O'Reilly SY (2005) Heterogeneous and metasomatized mantle recorded by trace elements in minerals of the Donghai garnet peridotites, Sulu UHP terrane, China. *Chem Geol* 221:243–259